ACS APPLIED MATERIALS & INTERFACES

Research Article

www.acsami.org

# Enhanced Bioactivity of Mg–Nd–Zn–Zr Alloy Achieved with Nanoscale $MgF_2$ Surface for Vascular Stent Application

Lin Mao,[†,‡,⊗] Li Shen,[§,⊗] Jiahui Chen,[§] Yu Wu,[‡,∥] Minsuk Kwak,[‡] Yao Lu,[‡] Qiong Xue,[‡] Jia Pei,[†] Lei Zhang,[†] Guangyin Yuan,*[,†] Rong Fan,*[,‡,⊥] Junbo Ge,[§] and Wenjiang Ding[†]

[†]National Engineering Research Center of Light Alloys Net Forming and State Key Laboratory of Metal Matrix Composite, Shanghai Jiao Tong University, Shanghai 200240, China

[‡]Department of Biomedical Engineering, Yale University, New Haven, Connecticut 06511, United States

[§]Shanghai Institute of Cardiovascular Diseases, Department of Cardiology, Zhongshan Hospital, Fudan University, Shanghai 200032, China

[∥]Department of Engineering Mechanics, Zhejiang University, Hangzhou 310027, China

[⊥]Yale Comprehensive Cancer Center, New Haven, Connecticut 06520, United States

**ABSTRACT:** Magnesium (Mg) alloys have revolutionized the application of temporary load-bearing implants as they meet both engineering and medical requirements. However, rapid degradation of Mg alloys under physiological conditions remains the major obstacle hindering the wider use of Mg-based implants. Here we developed a simple method of preparing a nanoscale $MgF_2$ film on Mg–Nd–Zn–Zr (denoted as JDBM) alloy, aiming to reduce the corrosion rate as well as improve the biological response. The corrosion rate of JDBM alloy exposed to artificial plasma is reduced by ~20% from 0.337 ± 0.021 to 0.269 ± 0.043 mm·y$^{-1}$ due to the protective effect of the $MgF_2$ film with a uniform and dense physical structure. The in vitro cytocompatibility test of $MgF_2$-coated JDBM using human umbilical vein endothelial cells indicates enhanced viability, growth, and proliferation as compared to the naked substrate, and the $MgF_2$ film with a nanoscale flakelike feature of ~200–300 nm presents a much more favorable environment for endothelial cell adhesion, proliferation, and alignment. Furthermore, the animal experiment via implantation of $MgF_2$-coated JDBM stent to rabbit abdominal aorta confirms excellent tissue compatibility of the well re-endothelialized stent with no sign of thrombogenesis and restenosis in the stented vessel.

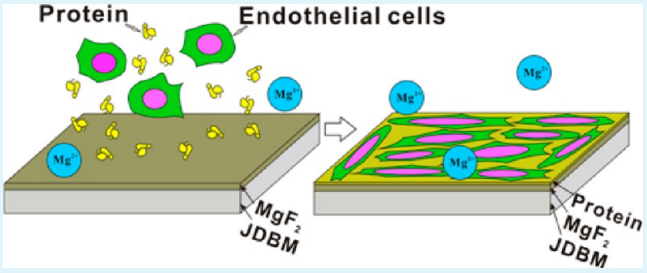


**KEYWORDS:** *magnesium alloy, surface modification, in vitro degradation, cytocompatibility, endothelialization*

## INTRODUCTION

Coronary artery disease remains the leading cause of both death and disability worldwide.[1,2] It happens when the arteries become narrowed owing to an accumulation of low-density lipoproteins in the intima.[3] Deploying stents in stenosed arteries is an effective way to expand the blocked vessel by overcoming the responses of acute elastic recoil and minimizing the vascular trauma after transluminal angioplasty. However, the clinical application of current permanent metallic stents such as stainless steel[4−6] and Ni–Ti shape-memory alloy[7,8] is challenged with several drawbacks, including long-term foreign body reaction, mechanical mismatch between the stented and nonstented vessel areas, delayed re-endothelialization, and high incidence of in-stent restenosis. Biodegradable and bioabsorbed stents that maintain the vessel structure in a limited period appear to provide an alternative approach to eliminate the complications associated with the long-term presence of permanent implants.

Magnesium is the fourth most abundant element in the human body. It is essential for the regulation of muscle contraction and human metabolism. Most importantly, the corrosion products of Mg alloys generated by the electrochemical reaction $Mg + 2H_2O \rightarrow Mg(OH)_2 + H_2$ are not deleterious to the surrounding tissues and can be absorbed/excreted by the human body.[9−11] Previous studies have shown great promise in using Mg alloys for biomedical application since the first Mg stent was successfully implanted into a preterm baby in 2004 by Zartner et al.[12] However, the uncontrolled corrosion rate of Mg alloys in physiological conditions limits their application as load-bearing biomedical scaffolds.[9,13] Mg alloys in chloride-containing environment are governed by the microgalvanic corrosion and easily suffer from pitting corrosion due to the nonequilibrium corrosion potential between the second phases/precipitated phases and the α-Mg matrix. We reported a type of Mg alloy Mg-2.5Nd-0.2Zn-0.4Zr (wt %, hereafter, denoted as JDBM) with highly homogeneous

Received: December 10, 2014
Accepted: February 23, 2015
Published: February 23, 2015




DOI: 10.1021/am5086885
ACS Appl. Mater. Interfaces 2015, 7, 5320−5330

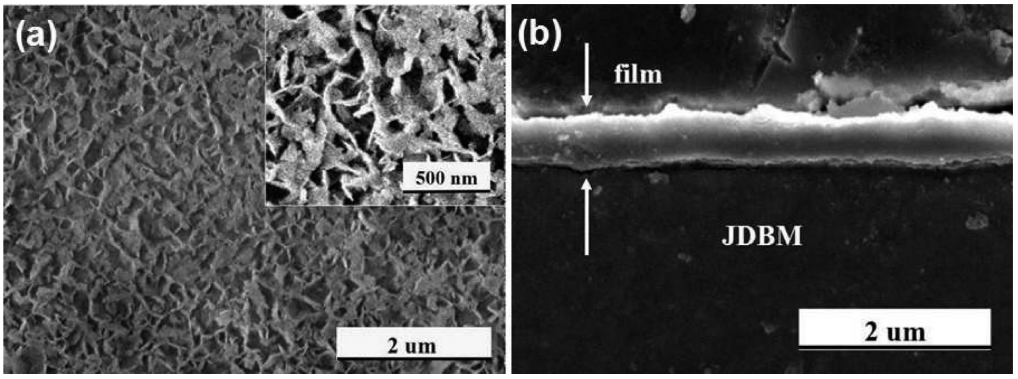


**Figure 1.** (a) Surface and (b) cross-sectional morphologies of the chemical conversion film on JDBM substrate treated in 0.1 M KF solution for 48 h. (inset) Detailed morphology of the conversion film with a nanoscale flakelike feature of ∼200−300 nm and a thickness of ∼0.8 $\mu$m shown in (b).

nanophasic degradation for biodegradable vascular stent application.[14,15] However, the surfaces of Mg-based stents are of high reactivity in physiological environment. The surface physicochemical properties of stent materials are believed to be of great importance for the initial protein deposition, surface-dependent cell behavior, and material-tissue interaction, and supposedly for later events such as re-endothelialization and inflammatory response during vascular remodeling process.

Critical advances in surface science and technology present an alternative avenue to improve the biocompatibility and bioefficacy of Mg-based implants. Current research of Mg alloys for biomedical applications mainly focus on elucidating the effect of different surface modifications on the improvement of corrosion resistance, cytocompatibility, and hemocompatibility.[16,17] The importance of cell behavior, especially that of endothelial cells, in terms of cell adhesion, proliferation, and alignment on the tissue-stent interface, is supported by the results of several investigations demonstrating that rapid-endothelialization decreases the incidences of thrombosis and in-stent restenosis.[6,18]

Herein, we developed an eco-friendly and simple method of preparing a nanoscale $MgF_2$ film on JDBM substrate through chemical conversion treatment of the Mg alloy in 0.1 M potassium fluoride (KF) solution. The in vitro degradation behaviors of JDBM substrate after surface modification and its cellular compatibility via direct and indirect cell assays were investigated to evaluate the feasibility of the modified JDBM alloy for biodegradable stent application. Animal studies were further carried out in abdominal aorta of New Zealand rabbits to evaluate the safety and efficacy of the modified JDBM stent in vivo. Results of this study indicate that the nanoscale $MgF_2$ film significantly enhances the performance of JDBM stent material including degradation rate and biocompatibility in vitro and in vivo and thus shows great potential for cardiovascular stent applications. To our knowledge, this is the first report of biodegradable Mg alloy with eco-friendly KF chemical treatment for cardiovascular stent application.

## EXPERIMENTAL SECTION

**Materials and Surface Modification.** The as-cast JDBM alloy was carried out by solution treatment (T4) at 540 °C for 10 h in argon atmosphere followed by water quench at 25 °C. After T4, the alloy was machined into cylindrical billets (Ø100 × 50 mm), extruded into bars (along the axial direction of the cylindrical billets, Ø20 mm) with an extrusion ratio of 25 at 350 °C, and annealed at 300 °C for 30 min. The specimen (Ø12 × 5 mm) was then ground, polished, and cleaned. JDBM alloy was chemically treated in 0.1 M KF solution for 48 h at room temperature to allow the formation of a dense conversion film, washed using running deionized water, and dried in a stream of warm air.

**Microstructure Characterizations.** The surface and cross-sectional morphologies of the conversion film were identified using field emission scanning electron microscope (FE-SEM, SIRION 200, FEI, America). The chemical composition of the film was characterized by X-ray diffraction (XRD, D/MAX 2000 V, Rigaku, Japan) with a Cu K$\alpha$ target and X-ray photoelectron spectroscopy (XPS, AXIS-ULTRA DLD, Kratos, Japan), respectively. The binding energies were calibrated using the binding energy of contaminant carbon ($C_{1S}$ = 284.8 eV).

**In Vitro Degradation Tests and Electrochemical Characterizations.** Immersion test and electrochemical measurements were performed according to ASTM-G31−72 in artificial plasma (6.8 g·$L^{-1}$ NaCl, 0.2 g·$L^{-1}$ $CaCl_2$, 0.4 g·$L^{-1}$ KCl, 0.1 g·$L^{-1}$ $MgSO_4$, 2.2 g·$L^{-1}$ $NaHCO_3$, 0.126 g·$L^{-1}$ $Na_2HPO_4$, 0.026 g·$L^{-1}$ $NaH_2PO_4$) at 37 °C and buffered at pH = 7.4. The volume of solution used for immersion test was calculated based on a volume-to-sample area ratio of 30 mL·$cm^{-2}$. After immersion for 10 d, the samples were cleaned for removing the corrosion products using a standard chromium trioxide ($CrO_3$) solution, rinsed with alcohol, and dried. The corrosion rate was calculated based on the weight loss of Mg samples. The volume of hydrogen evolution generated by Mg alloy degradation was measured according to the procedure in ref 19.

The electrochemical behavior of Mg substrate was evaluated in artificial plasma at 37 °C using a PARSTAT 2273 advanced electrochemical system (Princeton Applied Research). A three-electrode electrochemical cell was used, with the saturated calomel electrode as a reference electrode, a platinum electrode as a counter electrode, and Mg substrate as a working electrode. The specimen area exposed to the electrolyte was 1 $cm^2$. The electrochemical impedance spectroscopy (EIS) measurement was performed from 100 mHz to 100 MHz with the amplitude of alternating current of 10 mV. Potentiodynamic polarization test was carried out at a scanning rate of 1 mV·$s^{-1}$.

**Indirect Cytotoxicity Evaluations.** Human umbilical vein endothelial cells (HUVECs) were adopted to evaluate the cytotoxicity of Mg alloys by indirect cell assay. Mg alloy extract was prepared using EBM (Lonza, Cat. No. CC-3156) serum-free medium with the sample surface area-to-cell culture medium volume ratio of 1.25 $cm^2$·$mL^{-1}$. The apoptosis and necrosis ratios were assessed with flow cytometry by staining HUVECs with YO-PRO-1 (Life Technologies-Invitrogen, Cat. No. Y3603) and propidium iodide (PI, SIGMA-Aldrich, Cat. No. P4170). HUVECs were stained with Phalloidin (Life Technologies-Invitrogen, Cat. No. A22282) and DRAQ5 (Cell Signaling Technology, Cat. No. 4084S) to identify cell morphologies. Proliferating HUVECs were monitored by BrdU incorporation into nuclei of dividing cells for 30 min, followed by BrdU Mouse mAb Labeling and Anti-Mouse IgG (H+L) Detection (Cell Signaling Technology, Cat. No. 6813).


DOI: 10.1021/am5086885
ACS Appl. Mater. Interfaces 2015, 7, 5320−5330

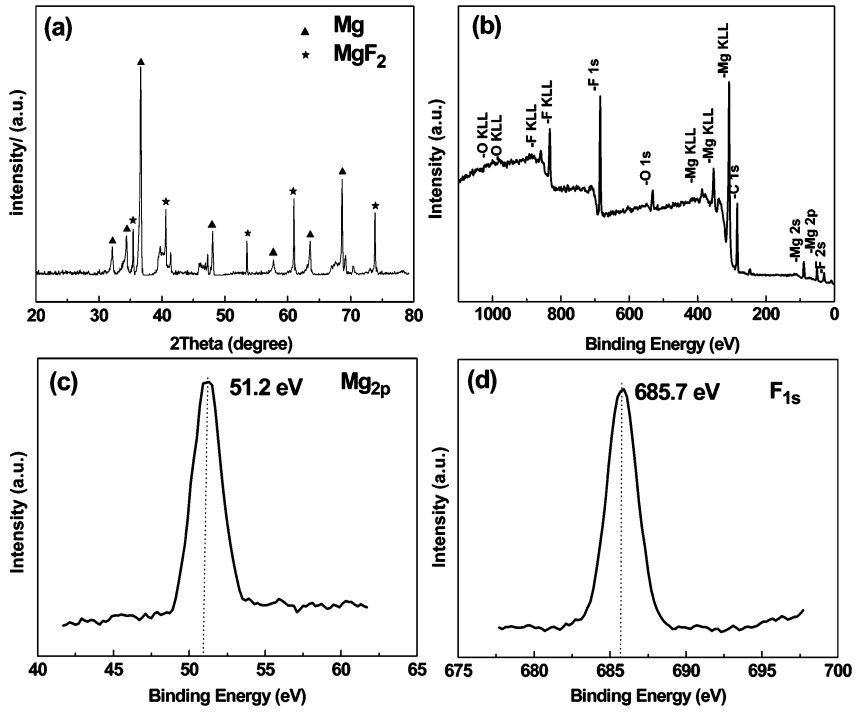


**Figure 2.** XRD pattern and XPS spectra for the conversion film obtained at 48 h of treatment of the JDBM alloy in KF solution. (a) XRD pattern, (b) XPS surface survey scan, (c) $Mg_{2p}$, (d) $F_{1s}$.

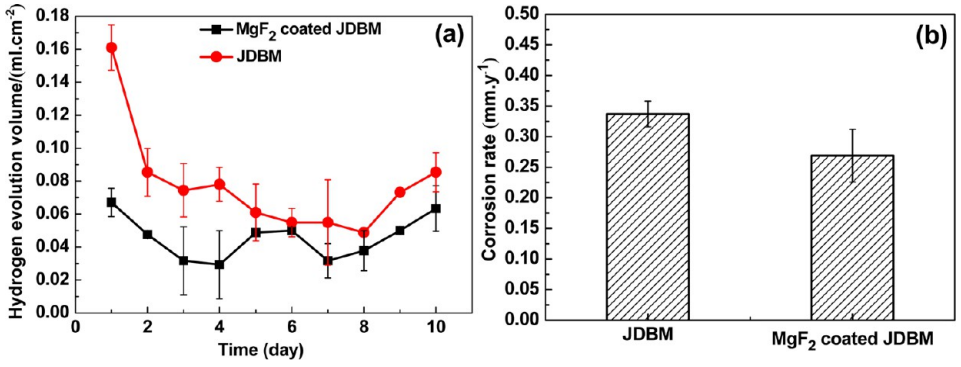


**Figure 3.** (a) $H_2$ evolutions and (b) corrosion rates for immersion of JDBM and $MgF_2$-coated JDBM substrates in artificial plasma for 10 d.

**Direct Cell Adhesion Experiments.** HUVECs were seeded onto the naked and coated JDBM substrates at a cell density of $2 \times 10^5$ cell·$mL^{-1}$ for a period of 24 and 48 h, respectively. The samples were then rinsed gently with phosphate buffer solution (PBS) three times, and the adherent cells were fixed, blocked, and stained with Phalloidin and DRAQ5 to evaluate the direct interaction of human endothelial cells with Mg substrates.

**Animal Experiments.** Animal experiments were approved by the Animal Ethics Committee of Zhongshan Hospital and conducted under the National Institutes of Health Guide for Care and Use of Laboratory Animals. Sex-unlimited, 3–4 months old, healthy, and clean New Zealand white rabbits weighing 2.5–3.5 kg were brought from the laboratory animal center of Zhongshan Hosptial, Fudan University, China.

JDBM stent with an original dimension of 2 × 14 mm was fabricated in Shanghai Jiao Tong University, China, and then treated with electrochemical polishing, followed by cleaning and drying. After that, surface modification was carried out by immersing JDBM stent in 0.1 M KF solution for 48 h to allow the conversion film formation on the surface of stent struts.

Animals were anaesthetized with a combination of 5% pentobarbital sodium (1–2 mL·$kg^{-1}$) by intravenous injection and implanted with Mg stents for different periods of 2, 7, and 28 d. Serial angiography and the follow-up in vivo angiography and intravascular ultrasound (IVUS) were performed to examine the safety and efficiency of biodegradable Mg alloy stents. Histologic examination of stented vessel via hematoxylin-eosin (HE) staining and SEM was used to determine the inflammatory response to the implant and the in-stent re-endothelialization process of biodegradable Mg alloy stent.

## RESULTS

**Surface Characterizations.** The surface and cross-sectional morphologies of the KF chemical conversion film on JDBM alloy are presented in Figure 1. A uniform and dense conversion film is successfully obtained on JDBM substrate (Figure 1a). The inset in Figure 1a shows the more detailed morphology of the conversion film with a nanoscale flakelike feature of ~200–300 nm. The conversion film with a thickness of ~0.8 $\mu$m bonds to the matrix strongly. The tape test was applied to test the adhesive ability of the conversion film to JDBM substrate. Result of this study shows that the adhesive strength can achieve classification 4B (the area of scratch is less than 5% of the total area of the film) according to ASTM D


DOI: 10.1021/am5086885
ACS Appl. Mater. Interfaces 2015, 7, 5320–5330

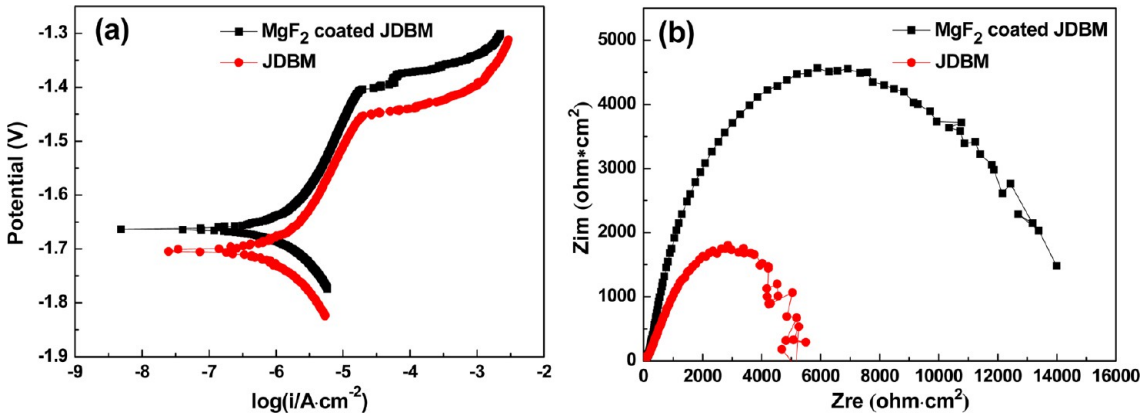


**Figure 4.** Electrochemical characterizations of JDBM and $MgF_2$-coated JDBM degradation process. (a) Potentiodynamic polarization curves. (b) Nyquist plots.

3359, indicating a strong adhesion of the film to JDBM substrate (Figure 1b).

The XRD pattern and XPS spectra for the conversion film after 48 h of treatment on JDBM alloy are obtained, as shown in Figure 2. $MgF_2$ phase is detected besides the $\alpha$-Mg phase from XRD pattern (Figure 2a). The full spectrum of XPS shows that the conversion film is mainly composed of O, F, and Mg elements (Figure 2b). The oxygen is suspected to originate from hydrocarbons and/or carbon oxide contamination in the environment. The $F_{1s}$ and $Mg_{2p}$ spectra are detected as single peaks (Figure 2c,d). The binding energies of 685.7 eV for F level and 51.2 eV for Mg level demonstrate the form of $MgF_2$ with reference to the standard database values.[20] The phase of the chemical conversion film detected by XPS is consistent with the analysis of XRD. Thus, it is reasonable to conclude that the KF conversion film on JDBM substrate corresponds to $MgF_2$.

**Degradation Tests and Electrochemical Measurements.** The in vitro corrosion performances of the naked and $MgF_2$-coated JDBM alloys were investigated by immersion tests comprising of hydrogen ($H_2$) evolution and weight loss in artificial plasma buffered at pH = 7.4 for 10 d at 37 °C. The volume of $H_2$ generated by the degradation of $MgF_2$-coated JDBM alloy is much less than that generated by the naked substrate during the investigated period, especially in the initial period (Figure 3a). This result is further supported by the degradation rate calculation, as shown in Figure 3b. The in vitro degradation rate of JDBM substrate measured by mass loss is reduced by ~20% from 0.337 ± 0.021 to 0.269 ± 0.043 $mm \cdot y^{-1}$ due to the protective effect of the $MgF_2$ film on the substrate surface. Both the tests of $H_2$ evolution and weight loss clearly indicate that the corrosion resistance of JDBM alloy can be improved by the KF chemical conversion treatment.

To quantify the electrochemical behavior of Mg substrate during the degradation process, we performed potentiodynamic polarization measurement to further investigate the naked and $MgF_2$-coated JDBM with regard to the corrosion current ($i_{corr}$) and potential ($E_{corr}$, Figure 4a). The potentiodynamic polarization curves of the two samples show the same trend: the $i_{corr}$ decreases by ~17% from 1.91 to 1.58 $\mu A \cdot cm^{-2}$ due to the protective effect of the $MgF_2$ film on the substrate (Table 1), indicating that JDBM alloy exhibits improved corrosion resistance after KF chemical conversion treatment. Furthermore, the calculation result of the reduced corrosion current (~17%) roughly agrees with the corrosion rate calculated by the weight loss (~20%) measurement. We also performed EIS measurements to further investigate the corrosion mechanism of Mg alloy exposed to artificial plasma. Generally, the high-frequency semicircle in Nyquist plot can be attributed to the charge transfer in combination with the corrosion products, while the low-frequency semicircle reveals the diffusion process through a porous layer.[21,22] In comparison with the naked substrate, the Nyquist plot of $MgF_2$-coated JDBM exhibits a single capacitive loop with an increased diameter (Figure 4b), reflecting that the $MgF_2$ film serves as a passivating film and an effective barrier layer with a low susceptibility to pitting corrosion on the surface during the initial degradation process.[23]

**Table 1. Corrosion Potential ($E_{corr}$) and Current ($i_{corr}$) of JDBM and $MgF_2$-Coated JDBM Tested by Potentiodynamic Polarization Measurement**

| samples | $E_{corr}$, V | $I_{Corr}$, $MA \cdot cm^{-2}$ | $R_p$, $\Omega \cdot cm^{-2}$ |
|---|---|---|---|
| JDBM | −1.70 | 1.91 | $8.72 \times 10^4$ |
| $MgF_2$-coated JDBM | −1.66 | 1.58 | $2.21 \times 10^5$ |

**Indirect Cell Cytotoxicity Assay.** To explore the cellular response to the corrosion products of degradable Mg alloys, we examined cell viability, morphology, and proliferation potential of human endothelial cells exposed to Mg extracts. HUVECs incubated in Mg extracts for a period of 24 h were double stained with YO-PRO-1 and propidium iodide (PI) and analyzed with flow cytometry to qualify the viability in terms of the apoptosis and necrosis ratios. The percentage of normal healthy cells for JDBM alloy increases from 69.5% to 89.4% after being coated with a protective $MgF_2$ film, indicating that the protective film on the surface, which is well-tolerated by HUVECs, effectively inhibits the JDBM alloy from releasing excess degradation ions via corrosion in cell culture medium (Figure 5a,b). The percentage of HUVECs in S phase (i.e., DNA replication phase) through 24 h of incubation was determined by 5-bromo-20-deoxy-uridine (BrdU) incorporation, and the proliferation potential of HUVECs (96.75 ± 12.14) cultured in the extract of coated JDBM is higher than that cultured in the naked JDBM extract (90.24 ± 9.66) and comparable to the negative control (Figure 5c). We also performed immunofluorescence characterization of HUVEC morphology by staining the cytoskeleton and nuclei. HUVECs spread and elongate in the Mg extracts and display a typical morphology of cobblestone, with no significant difference in morphology as compared to the negative control cells (Figure


DOI: 10.1021/am5086885
ACS Appl. Mater. Interfaces 2015, 7, 5320−5330

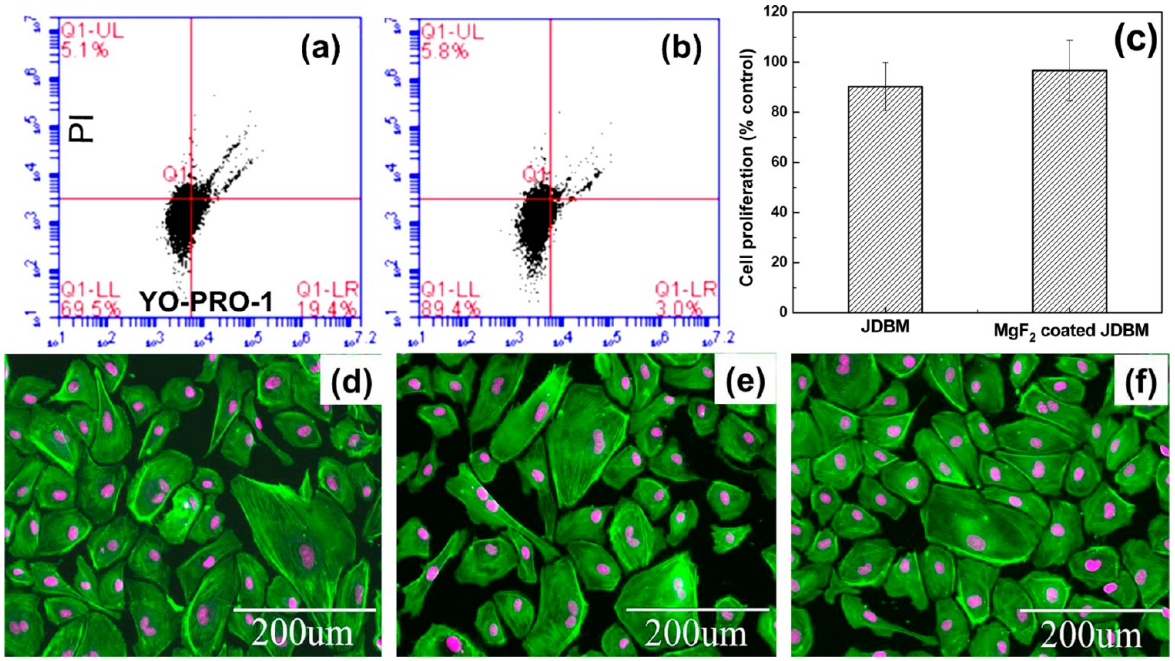


**Figure 5.** In vitro cytocompatibility tests of Mg alloy extracts on human endothelial cells. The ratio of apoptotic or necrotic cells is analyzed by flow cytometry on HUVECs treated with (a) JDBM and (b) $MgF_2$-coated JDBM extracts for 24 h. (c) Proliferation ratio of HUVECs cultured in JDBM and $MgF_2$-coated JDBM extracts for 24 h as compared to the negative control. Immunofluorescence images showing the morphology of HUVACs cultured in (d) normal cell culture medium and treated with (e) JDBM and (f) $MgF_2$-coated JDBM extracts for 24 h. The cells were fixed, penetrated, and stained for cytoskeleton (phalloidin 532 nm: green) and nuclei (DRAQ5 635 nm: purple).

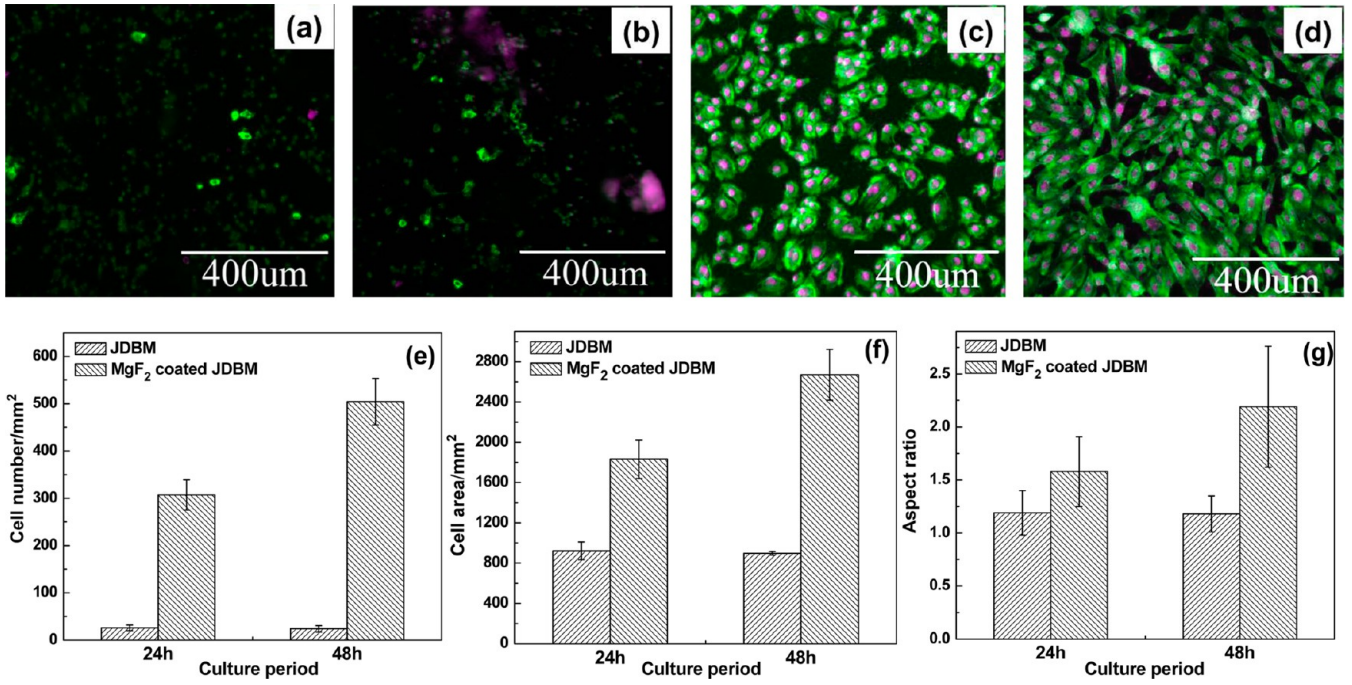


**Figure 6.** Cell attachment and elongation on Mg alloy substrates. HUVECs were seeded directly on (a, b) JDBM and (c, d) $MgF_2$-coated JDBM substrates and cultured for 24 and 48 h. The adherent cells were fixed, penetrated, and stained for cytoskeleton (phalloidin 532 nm: green) and nuclei (DRAQ5 635 nm: purple). Statistical analysis of the adherent cells in terms of (e) cell number, (f) mean cell area, and (g) mean aspect ratio of all the adherent HUVECs grown on the surfaces of JDBM and $MgF_2$-coated JDBM substrates.

5d–f). In brief, the indirect cell cytotoxicity cell assay indicates that primary human endothelial cells show enhanced viability and proliferation potential in modified JDBM extract as compared to that incubated in the naked substrate extract.

**Direct Cell Adhesion Experiment.** To evaluate the direct response of human endothelial cells to the naked and $MgF_2$-coated JDBM alloy, HUVECs suspension at the cell density of $2 \times 10^5$ cell·$mL^{-1}$ was seeded onto the substrates. The two Mg alloys with different physicochemical properties give rise to quite significant differences in terms of cell adhesion, spreading, and proliferation (Figure 6a–d). A few cells are observed on the naked JDBM surface after 24 h of culture, while the


DOI: 10.1021/am5086885
ACS Appl. Mater. Interfaces 2015, 7, 5320–5330

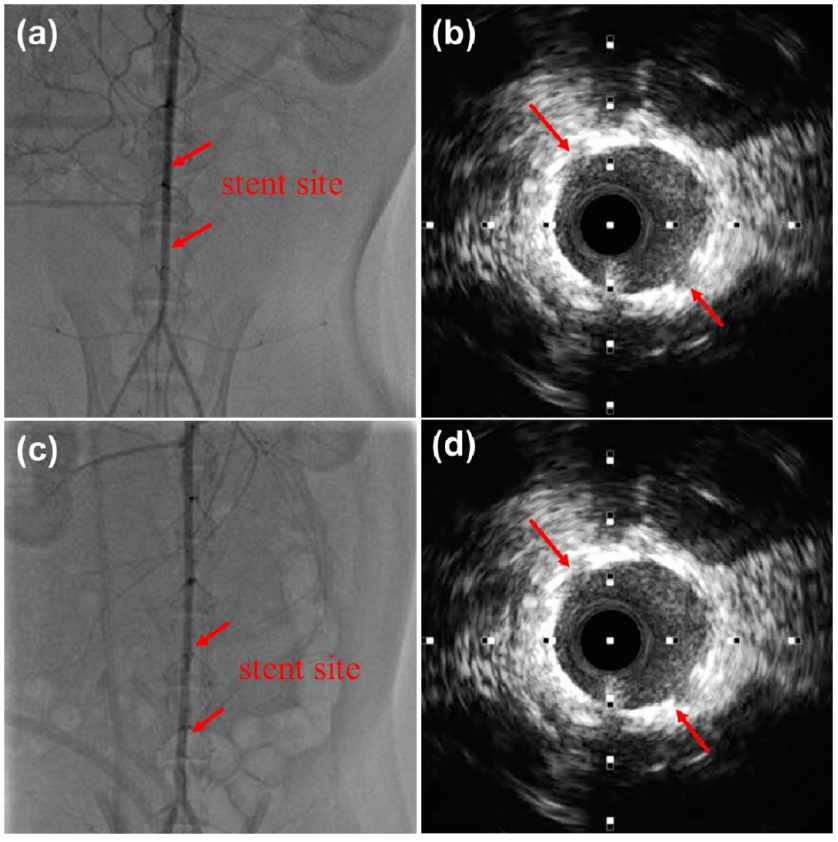


**Figure 7.** Four-week follow-up angiographic and the corresponding IVUS images of the abdominal aorta after (a, b) JDBM and (c, d) $MgF_2$-coated JDBM stent implantation. Note the longitudinal reconstruction of stented vessel and stent struts (arrow heads) at four-week implantation with an absence of in-stent restenosis and neointimal hyperplasia.

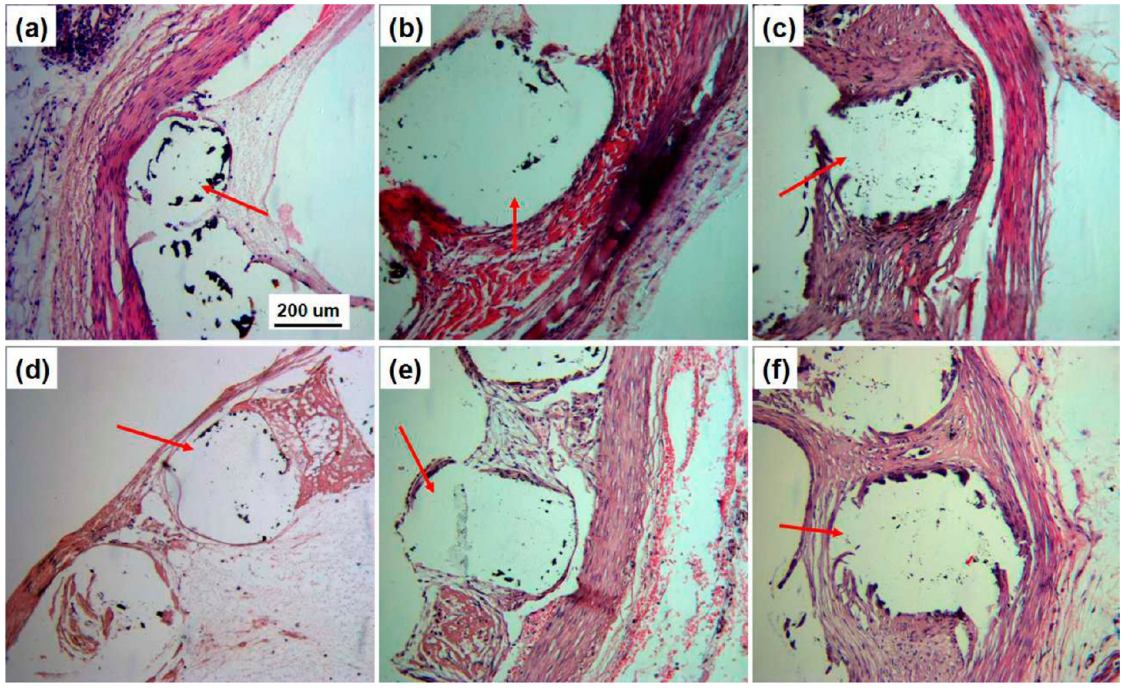


**Figure 8.** HE staining images of the stented arteries showing compromised inflammation reactions and neointimal coverage on the JDBM and $MgF_2$-coated JDBM struts in the period of (a, d) 2 d, (b, e) 7 d, and (c, f) 28 d of implantation. The white boxes (arrow heads) indicating the stent struts apposed to the vessel wall.

adhesive cell density increases distinctly on the substrate of modified JDBM with a nanoscale flakelike $MgF_2$ surface. We extended the culture period to 48 h and observed obvious cell proliferation and elongated cell configuration with pseudopo-



DOI: 10.1021/am5086885
*ACS Appl. Mater. Interfaces* 2015, 7, 5320−5330

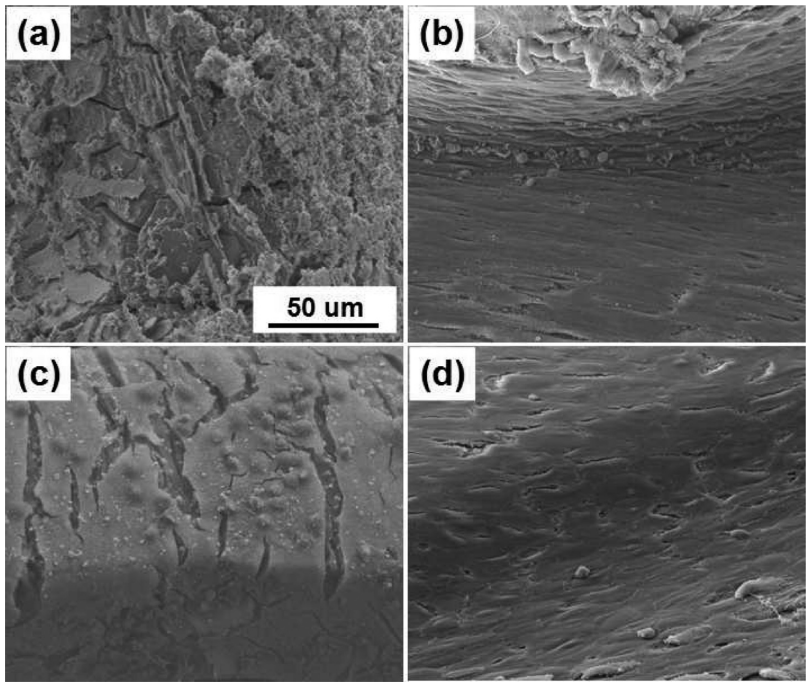


**Figure 9.** SEM images showing neointimal coverage of (a, b) JDBM stent and (c, d) $MgF_2$-coated JDBM stent after 7 and 28 d of implantation. Complete neointimal coverage on the modified struts post-stenting can be finished after 28 d of implantation, and few inflammatory cells are visible in the endothelialized stents.

dium well-adhered to each other on the surface of modified JDBM, and the cell alignment is similar to those cultured on normal tissue culture plate, indicating that the $MgF_2$ film with a nanoscale flakelike feature of ~200−300 nm presents much more favorable surface for endothelial cell adhesion, spreading, and alignment. However, very few HUVECs adhere on the naked JDBM substrate, and they appear to be rounded with inefficient cell spreading, indicating that rapid degradation made the naked JDBM substrate difficult to support the adhesion and growth of primary endothelial cells. Quantitative analysis of cell number, surface area, and aspect ratio of HUVECs grown on $MgF_2$-coated JDBM was analyzed by a high-content image analysis program (Cell prolifer 2.0, the Broad institute of MIT, Figure 6e−g). The adhesive ability of HUVECs is significantly improved as JDBM substrate is coated with $MgF_2$ film. We also observed that the mean cell number, cell area, and aspect ratio of HUVECs increase significantly ranging from 480 ± 50 to 788 ± 77 cell·$mm^{-2}$, from 1832.89 ± 192.75 to 2670.32 ± 253.16 $\mu m^2$, and from 1.58 ± 0.33 to 2019 ± 0.57, respectively, as endothelial cells were cultured on the modified JDBM substrate for 24 to 48 h of incubation. The statistics results confirm the morphological observation that the nanoscale flakelike $MgF_2$ offers a more favorable surface for adhesion, spreading, and proliferation of HUVECs and potentially aids in endothelialization of the stent into the denuded artery.

**In Vivo Angiography and Intravascular Ultrasound Findings.** In a previous study, we demonstrated that the JDBM stent with excellent radial strength and compliance can be completely expanded and well-apposed to the vessel wall, with no sign of early recoil or fracture at the initial implantation.[14] Here we further performed in vivo angiography and the follow-up IVUS to investigate the biosafety and efficacy of biodegradable JDBM and $MgF_2$-coated JDBM stents in rabbit abdominal aorta after implantation for 28 d (Figure 7). The angiography images show no thrombosis and serious in-stent restenosis in the naked and $MgF_2$-coated JDBM stents (Figure 7a,c), demonstrating that both the naked and modified stents are safe and efficient in vivo. The follow-up IVUS was used to evaluate the expansion level, initial hyperplasia degree, and the occurrences of thrombosis at 28 d post implantation, as shown in Figure 7b,d. Both the stents are well-apposed to the vessel wall with no evidence of strut fracture and in-stent restenosis, reflecting acceptable mechanical durability and excellent tissue compatibility of the biodegradable stents after 28 d of degradation in vivo. Meanwhile, we observed a thin layer of endothelium on the in-stent surface of the two stent struts at 28 d post implantation (Figure 7b,d).

**Histologic Observation and in-Stent Endothelialization.** We further performed HE staining to assess inflammatory response to biodegradable JDBM and $MgF_2$-coated JDBM stents in vivo (Figure 8). Histologic observation reveals compromised inflammation reactions with fewer inflammatory cell accumulation around $MgF_2$-coated JDBM stent and a thin continuous layer of neo-endothelium coverage on the in-stent surface in the period of 2 d of implantation, while increased inflammatory cells appears in the vicinity of the naked JDBM stent with partial coverage of neo-endothelium in all the three periods post implantation. A continuous and complete endothelium layer lines on the modified stent-supported artery after 28 d of implantation, indicating that $MgF_2$ film aids in the re-endothelialization process of JDBM stent into the denuded artery. The attenuation of the accumulation of inflammatory cells and the minor inflammatory reaction in the vicinity of $MgF_2$-coated JDBM stent can be reasonably attributed to the improved re-endothelialization process on the in-stent surface, which has been demonstrated as the main underlying mechanism of late stent thrombosis.[24]

We also investigated the distal segment of the stented artery to identify in-stent endothelialization process at various periods


DOI: 10.1021/am5086885
ACS Appl. Mater. Interfaces 2015, 7, 5320−5330

after implantation via SEM. A thin and noncontinuous endothelium layer covers on the surface of JDBM stent with inflammatory cell accumulation locally at 7 d post stenting, while obvious neointimal coverage on $MgF_2$-coated JDBM struts and fewer inflammatory cells are visible on the endothelialized stent (Figure 9a,c), reflecting that the nanoscale flakelike $MgF_2$ film has the potential to provide a favorable surface suitable for the initial adhesion, proliferation, migration, and alignment of host endothelial cells. Results of this study, which correspond well with the finding of direct cell adhesion on Mg substrates (Figure 6), also indicate that complete neointimal coverage on $MgF_2$-coated JDBM struts post-stenting can be achieved in the initial four weeks post implantation as shown in Figure 9d. Hence, we can conclude that $MgF_2$-coated JDBM stent causes less inflammatory reaction in the early implantatin periods and also accelerates the re-endothelialization possess after stenting compared with the naked JDBM stent. The major improvement in endothelialization process and inflammation inhibition can be reasonably attributed to the reduced degradation rate and enhanced biological activity of the $MgF_2$ film on JDBM substrate surface, which demonstrates great potential of the nanoscale flakelike $MgF_2$ coating for cardiovascular stent applications.

## DISCUSSION

Magnesium (Mg) alloys appear to be promising candidates as temporary structural biomaterial for orthopedic implants or cardiovascular stent applications due to the intriguing combination properties of biocompatibility, biodegradability, and mechanical performance.[12,14] Mg-based implants are expected to be completely degraded in physiological environment, and the degradation products should not pose threats to the surrounding tissues.[12] The temporary presence of Mg-based implants in the human body provides an avenue to overcome the complications associated with permanent implants through avoiding the long-term foreign body reaction and endothelial dysfunction. However, Mg alloys typically have low corrosion resistance under physiological conditions associated with a rapid release of degradation ions, the formation of extensive gas cavities, and early loosening of the implants, causing complete failure of the implant before the tissue has sufficiently healed.[9,25,26]

Surface modification such as surface coating/film is of great significance and is a very attractive way to control the high corrosion rate as well as improve the biocompatibility of Mg and its alloys.[16,17] Chemical conversion film is an in situ grown coating that is produced by chemical or electrochemical treatment of a metal to produce a superficial layer that is chemically bonded to the substrate. Mg is known to be the most resistant metal to fluoride-conditioned solutions due to the formation of a passivating protective layer on the metal surface.[27] In this study, we developed an eco-friendly surface modification to produce a fluoride film on the JDBM substrate with the reaction of this Mg alloy and 0.1 M KF solution for a period of 48 h. This conversion film is formed by the following chemical reaction. The $MgF_2$ film is grown directly on the metal substrate and is supposed to possess strong adhesive ability to the Mg alloy via atomic bond.

$$Mg^{2+} + 2F^- \rightarrow MgF_2$$

The variation of the corrosion rates between the naked and modified JDBM alloys is attributed to the protective effect of $MgF_2$ film, which shows a uniform and dense physical structure. The integrity of this barrier film enhances the corrosion resistance of JDBM alloy by preventing the substrate from severe eroding to release excess degradation ions in physiological environment and, consequently, leads to enhancement in cellular response to the extract of $MgF_2$-coated JDBM substrate (Figure 5). However, the conversion film $MgF_2$ is insoluble in aqueous solution but can be dissolved gradually in $Cl^-$-containing environment. The JDBM substrate begins to degrade when the electrolyte penetrates through the protective $MgF_2$ film. Mg and its alloy are known to be highly reactive in chloride ion-rich solution. The standard electrochemical potential of Mg is −2.4 V (−1.5 V in aqueous solutions due to the formation of a barrier film $Mg(OH)_2$).[28] Generally, the second phases/precipitated phases in Mg alloys are more noble than the $\alpha$-Mg matrix, and hence, typical galvanic corrosion is the prominent mechanism in Mg alloys due to the non-equilibrium corrosion potential between different constituent phases, resulting in severe pitting/local corrosion in Mg substrates. However, the main precipitated phase of extruded JDBM alloy is $Mg_{12}Nd$, and the potential difference between $Mg_{12}Nd$ and the $\alpha$-Mg matrix is very slight (~25 mV),[14,29] which is anticipated to slow down the galvanic corrosion and consequently improve the homogeneous degradation of the substrate. Thus, the uniform corrosion behavior of the JDBM substrate, which can avoid local stress concentration and rapid decrease of mechanical strength of the implants, is highly desired for load-bearing medical device applications.

The surface physicochemical properties of implanted materials have significant effects upon production of local microenvironments, which profoundly influence cellular behavior in terms of adhesion, spreading, intracellular signaling, and differentiation potential.[3] Because of rapid kinetics, biomaterials and medical devices exposed to blood immediately acquire a layer of plasma and extracellular matrix proteins prior to interacting with host cells.[30] Although the corrodibility of Mg alloys are desirable for temporary biodegradable implant applications, the surfaces of Mg-based implants are highly reactive in physiological medium, which may have adverse effect on the formation of a transient provisional matrix on and around the implants as well as the outcome of the subsequent cell colonization.[31,32] Hence, further surface modifications are necessary with respect to the improvement of surface stability and biological compatibility. Existing data supporting the positive role of nanostructured metals in biological application suggest that nanoscale modification of implant surface has the potential to yield a faster and more stable integration of biomedical implants with greater biological activity.[33] It is reported that a laser-nanostructured polystyrene surface with a periodic feature of 200−430 nm can significantly enhance adhesion and proliferation of mammalian cells,[34] and the topography cues down to 200 nm have adverse effect on primary corneal and human corneal epithelial cell (SV40-HCEC) proliferation.[35] In this work, we prepared a $MgF_2$ film with a nanoscale flakelike feature of ~200−300 nm on JDBM substrate surface with a simple chemical conversion treatment and demonstrated that the $MgF_2$ film favors HUVECs deposition, proliferation, and alignment and potentially aids in re-endothelialization of the implant into the denuded artery. Enhanced endothelial cell adhesion, proliferation, and alignment has been suggested as a method for increasing efficacy of


DOI: 10.1021/am5086885
ACS Appl. Mater. Interfaces 2015, 7, 5320−5330

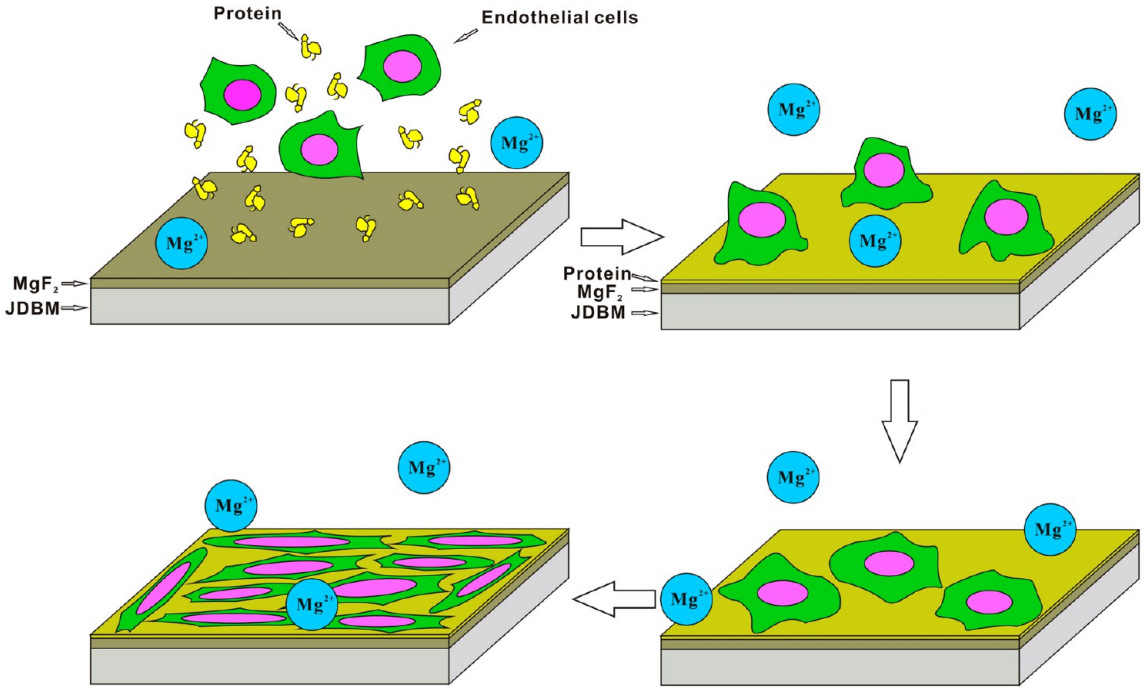


**Figure 10.** Schematic diagrams illustrate the processes of protein deposition and the subsequent consequences of endothelial cell adhesion, spreading, proliferation, and alignment on biodegradable $MgF_2$-coated JDBM stent.

vascular stents through preventing thrombosis and reducing inflammatory response.[18] To extend the in vitro findings, we further assessed the safety and efficacy of $MgF_2$-coated JDBM stent in animal model and confirmed accelerated in-stent re-endothelialization and excellent tissue compatibility of the modified vascular stent with the stented artery.

Figure 10 illustrates schematic diagrams of the processes of endothelial cell adhesion and the subsequent consequences of cell proliferation, migration, and alignment on biodegradable $MgF_2$-coated JDBM stent based on the in vitro and in vivo results. In the very initial process of implants exposed to blood, interaction of the modified JDBM stent and blood occurs with protein adsorption to the substrate surface, and development of the serum-rich plasma and extracellular matrix proteins such as albumin, fibronectin, laminin, vitronectin, and fibrinogen deposited onto the surface provides endothelial cells with a means of attaching via surface receptors.[32] Subsequent cell adhesion and cytoskeletal rearrangement are largely determined by the surface-dependent absorbed protein layer. Available data concerning surface structuring at nanoscale that are more effective in dictating protein adsorption and ultimately determining the biochemical characteristics of the layer are described.[34,36] Endothelial behaviors including proliferation, migration, and alignment are of great significance for the interaction of native endothelial cells with implanted scaffolds, which are strongly associated with the ultimate outcome of implants. It is reported that the faster the vascular stent is restored with an endothelium layer, the less likely the incidences with in-stent restenosis and thrombosis will occur.[18] In our in vitro cell assays, we observed enhanced cell adhesion, proliferation, and alignment on $MgF_2$-coated JDBM substrate (Figure 6), and the in vivo results confirmed accelerated in-stent endothelialization process and reduced inflammation in the vicinity of modified JDBM stent (Figures 8 and 9).

It is still uncertain what material surface characteristics are critical in mediating cellular responses and host-material reactions. Much effort has been focused on the improvement of surface bioactivity of implantable scaffolds through coating of the implant with biologically active molecules such as peptides, antibodies, and growth factors to improve cell survival, function, and the ultimate success of implantable devices.[37−40] On the basis of the finding that the nanoscale flakelike $MgF_2$ film with the feature size of ∼200−300 nm presents a much more favorable environment for endothelial cell adhesion, proliferation, and alignment, our studies suggest that incorporation of surface physicochemical properties such as substrate composition, surface feature, size, and shape also needs to be considered in the design and fabrication of medical devices. In summary, the surface of vascular implants must be engineered to improve initial endothelial cell adhesion, proliferation, migration, and alignment. On the basis of the in vitro and in vivo evaluations, we conclude that the degradation products of $MgF_2$-coated JDBM substrate have good biocompatibility with human endothelial cells and that the nanoscale flakelike $MgF_2$ film offers a favorable surface for human endothelial cell adhesion, proliferation, and alignment. Thus, the preparation of $MgF_2$ film, along with its nanoscale flakelike morphology, offers promising future for potential use in cardiovascular stent applications.

## CONCLUSIONS

We have prepared a nanoscale $MgF_2$ film on JDBM alloy with a simple chemical conversion treatment. The $MgF_2$ film shows a uniform and dense physical structure and contributes to reducing the corrosion rate of JDBM alloy exposed to artificial plasma by ∼20% from 0.337 ± 0.021 to 0.269 ± 0.043 $mm{\cdot}y^{-1}$. A systematic study of in vitro cytocompatibility shows that $MgF_2$-coated JDBM in comparison with the naked substrate has minimal negative effect on HUVECs viability, growth, and proliferation, and the $MgF_2$ film with a nanoscale flakelike


DOI: 10.1021/am5086885
ACS Appl. Mater. Interfaces 2015, 7, 5320−5330

feature of ~200−300 nm offers a much more favorable surface for endothelial cell adhesion, proliferation, and alignment. Furthermore, JDBM vascular stent coated with $MgF_2$ film implanted in rabbit abdominal aorta confirms excellent tissue compatibility of the well re-endothelialized stent with no sign of thrombogenesis and restenosis in the stent-supported vessel. Therefore, the nanoscale flakelike $MgF_2$ film exhibits significantly enhanced performance of JDBM alloy with regard to degradation rate and biocompatibility and shows great potential for cardiovascular stent applications.

## AUTHOR INFORMATION


### Corresponding Authors

*E-mail: gyyuan@sjtu.edu.cn. (G.Y.Y.)
*E-mail: rong.fan@yale.edu. (R.F.)


### Author Contributions

L.M. and G.-Y.Y. designed experiments for materials synthesis, surface modification, and degradation characterizations. L.M. and R.F. designed the in vitro cell assays. L.M., Y.W., and Q.X. performed in vitro cell assay experiments and analyzed data. L.S. and J.-H.C. performed the animal experiments, the relevant data collection, and data analysis. All the authors contributed to the writing of manuscript.

### Author Contributions

⊗L.M. and L.S. contributed equally to this work.

### Notes

The authors declare no competing financial interest.

## ACKNOWLEDGMENTS

This work was supported by the Yale University new faculty startup fund (PI: R.F.). Research at Shanghai Jiao Tong University was supported by the National Key Technology R&D Program of the Ministry of Science and Technology (2012BAI18B01), China Postdoctoral Science Foundation funded project (2012M520892). This project was also supported by the National Basic Research Program ("973" Program) of China (2011CB503905) and the National Natural Science Foundation of China (81370323 and 11402227).

## REFERENCES


(1) Go, A. S.; Mozaffarian, D.; Roger, V. L.; Benjamin, E. J.; Berry, J. D.; Blaha, M. J.; Dai, S.; Ford, E. S.; Fox, C. S.; Franco, S. Heart Disease and Stroke Statistics–2014 Update: A Report from the American Heart Association. *Circulation* **2014**, *129*, 399−410.

(2) Liu, M. B.; Wang, W.; Zhou, M. G. Trend Analysis on the Mortality of Cardiovascular Diseases from 2004 to 2010 in China. *Chin. J. Epidemiol.* **2013**, *34*, 985−988.

(3) Witztum, J. L.; Steinberg, D. Role of Oxidized Low Density Lipoprotein in Atherogenesis. *J. Clin. Invest.* **1991**, *88*, 1785.

(4) Harbuzariu, A.; Dragomir-Daescu, D.; Gooden, J.; Holmes, D.; Simari, R.; Sandhu, G. New Duplex-alloy Bare Metal Stent Enables Magnetic Capture of Endothelial Cells and Reduces Neointimal Response to Injury. *J. Am. Coll. Cardiol.* **2012**, *59*, E59−E59.

(5) Kaiser, C.; Galatius, S.; Erne, P.; Eberli, F.; Alber, H.; Rickli, H.; Pedrazzini, G.; Hornig, B.; Bertel, O.; Bonetti, P. Drug-eluting Versus Bare-metal Stents in Large Coronary Arteries. *New Engl. J. Med.* **2010**, *363*, 2310−2319.

(6) Yang, Z.; Wang, J.; Luo, R.; Maitz, M. F.; Jing, F.; Sun, H.; Huang, N. The Covalent Immobilization of Heparin to Pulsed-plasma Polymeric Allylamine Films on 316L Stainless Steel and the Resulting Effects on Hemocompatibility. *Biomaterials* **2010**, *31*, 2072−2083.

(7) Trepanier, C.; Leung, T.; Tabrizian, M.; Yahia, L. H.; Bienvenu, J. G.; Tanguay, J. F.; Piron, D.; Bilodeau, L. Preliminary Investigation of the Effects of Surface Treatments on Biological Response to Shape Memory NiTi Stents. *J. Biomed. Mater. Res.* **1999**, *48*, 165−171.

(8) Trepanier, C.; Tabrizian, M.; Yahia, L. H.; Bilodeau, L.; Piron, D. L. Effect of Modification of Oxide Layer on NiTi Stent Corrosion Resistance. *J. Biomed. Mater. Res.* **1998**, *43*, 433−440.

(9) Staiger, M. P.; Pietak, A. M.; Huadmai, J.; Dias, G. Magnesium and its Alloys as Orthopedic Biomaterials: a Review. *Biomaterials* **2006**, *27*, 1728−1734.

(10) Zeng, R.; Dietzel, W.; Witte, F.; Hort, N.; Blawert, C. Progress and Challenge for Magnesium Alloys as Biomaterials. *Adv. Eng. Mater.* **2008**, *10*, B3−B14.

(11) Zhang, X.; Li, X.-W.; Li, J.-G.; Sun, X.-D. Preparation and Characterizations of Bioglass Ceramic Cement/Ca−P Coating on Pure Magnesium for Biomedical Applications. *ACS Appl. Mater. Interfaces* **2013**, *6*, 513−525.

(12) Zartner, P.; Cesnjevar, R.; Singer, H.; Weyand, M. First Successful Implantation of a Biodegradable Metal Stent into the Left Pulmonary Artery of a Preterm Baby. *Catheter. Cardiovasc. Interventions* **2005**, *66*, 590−594.

(13) Witte, F.; Kaese, V.; Haferkamp, H.; Switzer, E.; Meyer-Lindenberg, A.; Wirth, C.; Windhagen, H. In vivo Corrosion of Four Magnesium Alloys and the Associated Bone Response. *Biomaterials* **2005**, *26*, 3557−3563.

(14) Mao, L.; Shen, L.; Niu, J.; Zhang, J.; Ding, W.; Wu, Y.; Fan, R.; Yuan, G. Nanophasic Biodegradation Enhances the Durability and Biocompatibility of Magnesium Alloys for the Next-Generation Vascular Stents. *Nanoscale* **2013**, *5*, 9517−9522.

(15) Eley, E., Next-Generation Vascular Stents. Chemistry World. 2013. http://www.rsc.org/chemistryworld/2013/08/biodegradable-vascular-stent-atherosclerosis.

(16) Ye, S. H.; Jang, Y. S.; Yun, Y. H.; Shankarraman, V.; Woolley, J. R.; Hong, Y.; Gamble, L. J.; Ishihara, K.; Wagner, W. R. Surface Modification of a Biodegradable Magnesium Alloy with Phosphorylcholine (PC) and Sulfobetaine (SB) Functional Macromolecules for Reduced Thrombogenicity and Acute Corrosion Resistance. *Langmuir* **2013**, *29*, 8320−8327.

(17) Zomorodian, A.; Garcia, M.; Moura e Silva, T.; Fernandes, J.; Fernandes, M.; Montemor, M. Corrosion Resistance of a Composite Polymeric Coating Applied on Biodegradable AZ31 Magnesium Alloy. *Acta Biomater.* **2013**, *9*, 8660−8670.

(18) Pislaru, S. V.; Harbuzariu, A.; Agarwal, G.; LATG, T. W. A. C.; Gulati, R.; Sandhu, N. P.; AA, C. M.; Kalra, M.; Simari, R. D.; Sandhu, G. S. Magnetic Forces Enable Rapid Endothelialization of Synthetic Vascular Grafts. *Circulation* **2006**, *114*, I-314−I-318.

(19) Song, G.; Atrens, A. Understanding Magnesium Corrosion—a Framework for Improved Alloy Performance. *Adv. Eng. Mater.* **2003**, *5*, 837−858.

(20) Moulder, J. F.; Stickle, W. F.; Sobol, P. E.; Bomben, K. D. *Handbook of X-ray Photoelectron Spectroscopy;* Perkin Elmer: Eden Prairie, MN, 1992; Vol. *40*.

(21) Deslouis, C.; Duprat, M.; Tulet-Tournillon, C. The Cathodic Mass Transport Process During Zinc Corrosion in Neutral Aerated Sodium Sulphate Solutions. *J. Electroanal. Chem. Interfacial Electrochem.* **1984**, *181*, 119−136.

(22) Park, J.; Macdonald, D. Impedance Studies of the Growth of Porous Magnetite Films on Carbon Steel in High Temperature Aqueous Systems. *Corros. Sci.* **1983**, *23*, 295−315.

(23) Brett, C.; Dias, L.; Trindade, B.; Fischer, R.; Mies, S. Characterisation by EIS of Ternary Mg Alloys Synthesised by Mechanical Alloying. *Electrochim. Acta* **2006**, *51*, 1752−1760.

(24) Christiansen, E. H.; Jensen, L. O.; Thayssen, P.; Tilsted, H.-H.; Krusell, L. R.; Hansen, K. N.; Kaltoft, A.; Maeng, M.; Kristensen, S. D.; Bøtker, H. E. Biolimus-Eluting Biodegradable Polymer-Coated Stent Versus Durable Polymer-Coated Sirolimus-Eluting Stent in Unselected Patients Receiving Percutaneous Coronary Intervention (SORT OUT V): a Randomised Non-Inferiority Trial. *Lancet* **2013**, *381*, 661−669.

(25) Choudhary, L.; Singh Raman, R. Magnesium Alloys as Body Implants: Fracture Mechanism under Dynamic and Static Loadings in a Physiological Environment. *Acta Biomater.* **2012**, *8*, 916−923.




DOI: 10.1021/am5086885
*ACS Appl. Mater. Interfaces* 2015, 7, 5320−5330

(26) Kannan, M. B.; Raman, R. In vitro Degradation and Mechanical Integrity of Calcium-Containing Magnesium Alloys in Modified-Simulated Body Fluid. *Biomaterials* **2008**, *29*, 2306−2314.
(27) Witte, F.; Fischer, J.; Nellesen, J.; Vogt, C.; Vogt, J.; Donath, T.; Beckmann, F. In vivo Corrosion and Corrosion Protection of Magnesium Alloy LAE442. *Acta Biomater.* **2010**, *6*, 1792−1799.
(28) Ambat, R.; Aung, N. N.; Zhou, W. Evaluation of Microstructural Effects on Corrosion Behaviour of AZ91D Magnesium Alloy. *Corros. Sci.* **2000**, *42*, 1433−1455.
(29) Coy, A.; Viejo, F.; Skeldon, P.; Thompson, G. Susceptibility of Rare-Earth-Magnesium Alloys to Micro-galvanic Corrosion. *Corros. Sci.* **2010**, *52*, 3896−3906.
(30) Anderson, J. M. Biological Responses to Materials. *Annu. Rev. Mater. Res.* **2001**, *31*, 81−110.
(31) Anderson, J. M.; McNally, A. K. In *Biocompatibility of Implants: Lymphocyte/Macrophage Interactions,* Seminars in immunopathology; Zimmerli, W., Ed.; Springer: Berlin, Germany, 2011; pp 221−233.
(32) Anderson, J. M.; Patel, J. D. Biomaterial-Dependent Characteristics of the Foreign Body Response and S. epidermidis Biofilm Interactions. *Biomaterials Associated Infection;* Moriarty, T. F., Zaat, S. A. J., Busscher, H. J., Eds.; Springer: Berlin, Germany, 2013; pp 119−149.
(33) Variola, F.; Brunski, J. B.; Orsini, G.; de Oliveira, P. T.; Wazen, R.; Nanci, A. Nanoscale Surface Modifications of Medically Relevant Metals: State-of-the Art and Perspectives. *Nanoscale* **2011**, *3*, 335−353.
(34) Rebollar, E.; Frischauf, I.; Olbrich, M.; Peterbauer, T.; Hering, S.; Preiner, J.; Hinterdorfer, P.; Romanin, C.; Heitz, J. Proliferation of Aligned Mammalian Cells on Laser-Nanostructured Polystyrene. *Biomaterials* **2008**, *29*, 1796−1806.
(35) Liliensiek, S. J.; Campbell, S.; Nealey, P. F.; Murphy, C. J. The Scale of Substratum Topographic Features Modulates Proliferation of Corneal Epithelial Cells and Corneal Fibroblasts. *J. Biomed. Mater. Res., Part A* **2006**, *79*, 185−192.
(36) Mendonça, G.; Mendonca, D.; Aragao, F. J.; Cooper, L. F. Advancing Dental Implant Surface Technology−from Micron-to Nanotopography. *Biomaterials* **2008**, *29*, 3822−3835.
(37) Dean, J., 3rd; Culbertson, K. C.; D'Angelo, A. M. Fibronectin and Laminin Enhance Gingival Cell Attachment to Dental Implant Surfaces in vitro. *Int. J. Oral Maxillofac. Implants* **1994**, *10*, 721−728.
(38) Yazici, H.; Fong, H.; Wilson, B.; Oren, E.; Amos, F.; Zhang, H.; Evans, J.; Snead, M.; Sarikaya, M.; Tamerler, C. Biological Response on a Titanium Implant-Grade Surface Functionalized with Modular Ppeptides. *Acta Biomater.* **2013**, *9*, 5341−5352.
(39) Liao, K.-H.; Lin, Y.-S.; Macosko, C. W.; Haynes, C. L. Cytotoxicity of Graphene Oxide and Graphene in Human Erythrocytes and Skin Fibroblasts. *ACS Appl. Mater. Interfaces* **2011**, *3*, 2607−2615.
(40) Yan, X.; Chen, J.; Yang, J.; Xue, Q.; Miele, P. Fabrication of Free-Standing, Electrochemically Active, and Biocompatible Graphene Oxide−Polyaniline and Graphene−Polyaniline Hybrid Papers. *ACS Appl. Mater. Interfaces* **2010**, *2*, 2521−2529.


DOI: 10.1021/am5086885
*ACS Appl. Mater. Interfaces* 2015, 7, 5320−5330